A Hybrid Optimization Approach for Pile Capacity Estimation Using Radial Basis Functions and Time-Dependent Variables

Shanwei Zhang
College of Design, Chongqing College of Finance and Economics, Yongchuan 402160, Chongqing, China
E-mail: 19936052713@163.com

Keywords: geotechnical engineering**,** predictive modeling**,** structural safety**,** soil properties, sensitivity analysis, time-dependent variables

Received: March 3, 2025

Since the pile and surrounding soil interact in complex, nonlinear ways and time-dependent geotechnical parameters play a significant role, accurately estimating the axial bearing capacity of driven piles is still a crucial but difficult part of geotechnical engineering. The new hybrid predictive framework proposed in this study combines two recent metaheuristic optimization algorithms, Leader Harris Hawks Optimization (LHHO) and Graylag Goose Optimization (GGO), with the Radial Basis Function (RBF) model. Through the incorporation of temporal variations, such as changes in soil resistance due to pore water pressure dissipation, that are commonly overlooked in conventional modeling approaches, the main goal is to improve the predictive accuracy and generalization capability of pile capacity models. By combining time-dependent variables with a correlation-based feature selection mechanism, this work is novel in that it enables the identification of the most important input parameters and the removal of redundant or unnecessary features. In comparison to actual pile load test data, the resulting hybrid models, known as RBGG and RBLH, perform better. During training, the RBLH model demonstrated high accuracy and reliability with an R^2 value of 0.986 and an RMSE of 183.680. In addition, sensitivity analysis showed that the most important factors affecting pile capacity are unit weight, soil cohesiveness, and pile length. With major ramifications for enhancing safety, decreasing uncertainty in construction procedures, and optimizing foundation design, the suggested methodology provides engineers with a strong, data-driven tool.

Povzetek: Prispevek obravnava nosilnost pilotov v povezavi z nelinearnimi interakcijami zemljine in časa. Predlaga hibridni pristop z radialnimi baznimi funkcijami (RBF), optimiziranimi z algoritmoma LHHO in GGO, ki vključuje časovno odvisne geotehnične spremenljivke.

1 Introduction

Pile foundations are structural components typically used when soil settlement is a critical consideration during the design phase or when surface soils are weak. In such cases, the structural load must be transferred to deeper soil layers. For geotechnical engineers, determining the ultimate bearing capacity of pile foundations is crucial, especially when considering the pile's role in load transmission. Some researchers have suggested that pile carrying capacity is a time-dependent variable, showing an upward trend after a certain period [1], [2], [3]. The geotechnical phenomenon known as 'pile setup' refers to the gradual increase in the ultimate bearing capacity of pile foundations. Pile setup is thought to be caused by the dissipation of excess pore water pressure (EPWP) produced during pile installation [4].

Additionally, it is generally acknowledged that this phenomenon progresses through three primary stages: aging, uniform EPWP dissipation, and non-uniform EPWP dissipation [5]. Several studies have found that setup significantly impacts side resistance, whereas relaxation shows little change or even a decrease in tip resistance [6], [7], [8]. Researchers have long been interested in predicting the time-dependent bearing capacity of pile foundations. Furthermore, considering pile setup in the design process could make the procedure more cost-effective.

Numerous studies predicting pile configuration using analytical or numerical models have been reported [9]. Skov and Denver's work [10] which aimed to determine an equation for predicting pile setup, is one of the most well-known studies in this field. To achieve this, several geotechnical characteristics were used to revise the setup equation. They also introduced a valid variable, known as the setup parameter (A), and presented a semi-empirical equation. Other researchers built upon this groundbreaking work. A study by Haque and Abu-Farsakh, for instance, examined the use of a nonlinear multivariable regression model to predict pile configuration. Although research employing this combination of methods has provided useful equations, pile placement remains a challenging problem due to the complex soil–pile interaction. As a result, regression analysis and analytical techniques may not be sufficient for making accurate predictions [11]. The effective use of

intelligent algorithms to model complex issues in geotechnical and civil engineering has been demonstrated in numerous studies in recent years [12], [13], [14]. Many researchers have highlighted the usefulness of these methods in predicting pile-related issues, such as lateral deflection, settlement, and pile capacity. Lee and Lee [15] examined the use of artificial neural networks (ANNs) for predicting pile bearing capacity. The developed model was validated using the results of in situ pile load tests. Ultimately, the error back-propagation neural network demonstrated strong performance, with a maximum prediction error below 25%. Shahin [16] modeled the axial capacity of pile foundations using intelligent computing. For this, 174 data points were used in an ANN approach to predict the axial capacity of driven piles and drilled shafts. The findings indicated that the ANN performed satisfactorily on the validation datasets for driven piles and drilled shafts, with correlation coefficients of 0.85 and 0.97, respectively. To evaluate pile carrying capacity, Samui [17] explored the use of the support vector machine, a powerful machine learning technique. For this, three inputs were considered: the number of bowls, mean normal stress, and penetration depth ratio. Ultimately, the developed model accurately predicted pile carrying capacity, using assessment criteria such as the correlation coefficient. In a different research, Momeni et al. [18] employed an ANN-based prediction model optimized with a genetic algorithm to predict pile carrying capacity, using data from 50 dynamic load tests. With a correlation coefficient of 0.99, the final data showed that the generated model accurately predicted the target value, which was very close to the actual value. Using regression and EPR-MOGA models, Alzabeebee et al. [19] investigated the relationship between internal friction angle and soil characteristics. The EPR-MOGA model demonstrated its efficacy in capturing intricate relationships in fine-grained soils by achieving high precision (R = 0.85–0.92), whereas linear regression showed moderate accuracy (R = 0.16–0.67). Kumar et al. [20] applied advanced ML models, including XGBoost, RF, GBM, and deep learning, to predict the bearing capacity of PGPN piles using 81 static load tests. XGBoost ($R^2 = 0.91$) and RF showed the best performance, while GBM underperformed. SHAP analysis and Taylor diagrams supported the model evaluation.

Pile foundations are crucial in modern geotechnical engineering, particularly when surface soils cannot support heavy structural loads. Traditional approaches for estimating pile bearing capacity rely on analytical or numerical models, which often fail to provide accurate estimations due to the complexities of soil-pile interaction and time-dependent soil behavior. This research introduces a novel framework that leverages advanced machine learning techniques, specifically the Radial Basis Function (RBF) model. This is coupled with state-of-the-art optimization algorithms, including Greylag Goose Optimization (GGO) and Leader Harris Hawks Optimization (LHHO). This unique combination improves prediction accuracy and reliability, addressing gaps in current methodologies. The novelty of this research lies in focusing on the inclusion of time-dependent variables in pile capacity prediction, which have often been neglected in conventional studies. While previous models have focused on static parameters like cohesion, friction, and soil unit weight, this work examines the dynamic development of pile capacity due to processes like pile setup, driven by EPWP dissipation. By incorporating time-dependent parameters such as average pile-soil friction and changes in soil resistance due to pore water pressure dissipation, this research develops a more comprehensive and adaptive predictive framework. Pile length, while not time-varying, is also included as a key geometric input in the model. In this study, the RBF model served as a tool to capture nonlinear relationships between input parameters and pile capacity. Model parameter fine-tuning was achieved using optimization algorithms such as GGO and LHHO, enhancing the model's accuracy. These optimization algorithms are inspired by the collective intelligence of natural systems, which self-organize and develop efficient search strategies to identify global optima in complex, multi-dimensional datasets. By combining these models and optimization techniques, the research achieves unprecedented precision in capturing the interaction between soil and pile parameters. The sensitivity analysis part of the paper shows the most influential parameters concerning the average cohesion, pile length, and soil specific weight on the capacity of the pile. In this way, engineers will be able to focus on the most relevant variables at the design stage in order to optimize material use with regard to cost. This research will add to the benefit of geotechnical engineering by providing a sound and data-based method for pile bearing capacity prediction. Its applications go beyond academia to the provision of practical tools for industry professionals to create more economical and safer designs of foundations, especially on poor soil classes or projects involved in long-term performance monitoring.

The selection of GGO and LHHO was motivated by their demonstrated performance in solving high-dimensional, nonlinear optimization problems with complex search landscapes. Both algorithms have gained attention in recent literature for their strong balance between global exploration and local exploitation, which is critical for effectively tuning the spread and weights in the RBF model. Specifically, LHHO offers enhanced adaptive leadership mechanisms that improve convergence speed, while GGO mimics collective geese flight behavior, which promotes diversity in the solution population and reduces the chance of local optima entrapment. Compared to traditional algorithms like Genetic Algorithm (GA) and Particle Swarm Optimization (PSO), both GGO and LHHO have shown lower sensitivity to parameter initialization and better generalization.

2 Dataset

The dataset comprises 229 pile load test records sourced from [21], [22], [23], [24], [25]. Each instance includes geotechnical and pile-related features, such as unit weight, cohesion, angle of internal friction, pile length, and time-

dependent parameters. Prior to model training, the dataset was carefully examined for missing values and outliers. No missing or anomalous values were detected. All numerical input features were normalized using Min-Max scaling to ensure uniform data ranges and improve model convergence.

The statistical characteristics of a few important input factors that affect the pile foundations' time-dependent bearing capacity are shown in Table 1. It gives the input indicators' lowest, maximum, average, and standard deviation values. The variability and character of the geotechnical parameters in this research study may be evaluated with the help of the following table.

- **Average Cohesion (0 to 475 kPa, Avg: 89.487 kPa):** Indicates how soil stickiness affects side friction (0 to 475 kPa, Avg: 89.487 kPa). Significant variation suggests a variety of soil types, which affect frictional resistance and, in turn, pile capacity.
- **Average Friction Angle (0 to 39 degrees, Avg: 19.554 degrees):** The shear strength of granular soils is influenced by the average friction angle, which ranges from 0 to 39 degrees and averages 19.554 degrees. Significant variation points to various soil stratifications that influence capacity variations over time.
- **Average Soil Specific Weight (0 to 29.54 kN/m³, Avg: 6.913 kN/m³):** This value influences pile bearing capacity and effective stress. When forecasting capacity, variability makes it evident that variations in pore water pressure are crucial.
- **Average Pile-Soil Friction (0 to 41 kPa, Avg: 14.955 kPa):** The pile-soil interaction is reflected in the average pile-soil friction, which ranges from 0 to 41 kPa and averages 14.955 kPa. Side resistance rises with high friction, which is crucial for sustained capacity improvements.
- **Flap Number (0 to 2291, Avg: 187.338):** This represents the inductive resistance of the soil (0 to 2291, average: 187.338). High variability lends credence to the possibility of a diverse foundation. High values indicate increased tip resistance.
- **Pile Area (0.006 to 34.02 m², Avg: 2.620 m²):** The load-bearing capability is directly impacted by this. In contrast to other factors, this trait has less of an association with time-dependent fluctuations.
- **Pile Length (1.000 to 207.00 m, Avg: 20.131 m):** Longer piles have deeper soil layers, which raises the possibility for tip bearing and side resistance when calculating capacity.
- **Pile Capacity (Output: 36.750 to 6789.00 kN, Avg: 2433.239 kN):** Because of the wide variations in circumstances, the pile capacity exhibits substantial fluctuation. A sensitivity study shows that cohesion, friction angle, and pile length are the main factors influencing the capacity projections.

All things considered, this analysis of Table 1 highlights the importance of including these factors in prediction models. Due to the observed variability, advanced optimization techniques are necessary to enhance the accuracy and reliability of pile capacity predictions, which are crucial for designing optimal pile foundations.

Table 1: The statistical properties of the input variable pile capacity

Variables		Indicators			
	Category	Min	Max	Avg	St. Dev.
Average Cohesion	Input	0.000	475.0	89.487	82.164
Average Friction	Input	0.000	39.0	19.554	15.500
Average soil Specific weight	Input	0.000	29.54	6.913	5.663
Average Pile-Soil Friction	Input	0.000	41.00	14.955	13.771
Flap Number	Input	0.000	2291.0	187.34	429.03
Pile Area	Input	0.006	34.02	2.620	5.246
Pile Length	Input	1.000	207.0	20.131	15.688
Pile Capacity	Output	36.750	6789.0	2433.24	1400.32

Fig. 1 presents a grouped 3D bar plot that illustrates the relationship between the input variables—Average Cohesion, Average Friction, Average Soil Specific Weight, Average Pile-Soil Friction, Flap Number, Pile Area, and Pile Length—and the output variable, Pile Capacity. This visualization demonstrates how changes in these key geotechnical parameters affect the predicted pile bearing capacity. It provides an overview of how these parameters influence the output, offering the opportunity for an in-depth analysis of the interactions between soil properties and pile characteristics, and their combined impact on the load-bearing capacity of pile foundations.

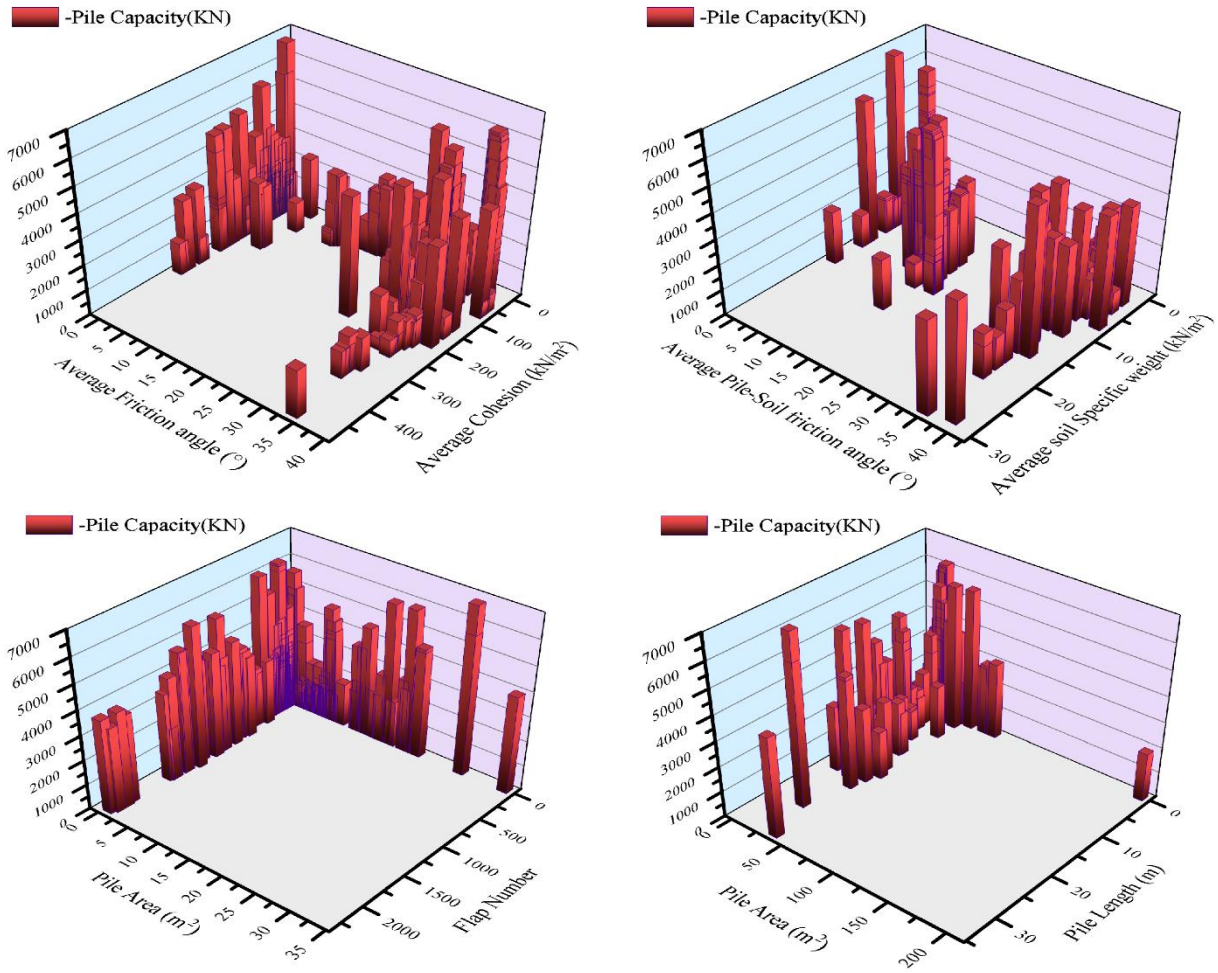

Figure 1: The grouped 3D bar plot displays the relationship between input and output

Fig. 2 shows the feature selection analysis of the dataset using important input variables with regard to the prediction of pile capacity. This indicates the percentage of contribution of every feature towards the model's performance. The most important feature is Pile Length, which has a score of 0.609; this is the most important factor in predicting the capacity of the pile. Flap Number is next, with the value 0.458, indicating a significant role in the variation of soil penetration resistance in determining the pile capacity. Other contributing variables to the model include Average Soil Specific Weight at 0.234, Pile Area at 0.145, and Average Friction at 0.137. The features with the least influence on predictive accuracy are Average Cohesion (0.135) and Average Pile-Soil Friction (0.016). This feature selection analysis helps in prioritizing the most influential factors in the development of models for pile capacity prediction, guiding further modeling and optimization efforts.

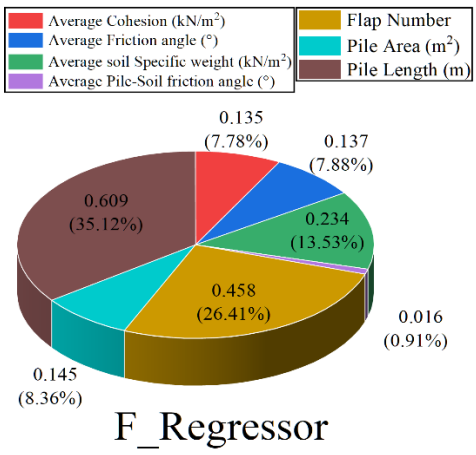

Figure 2: The feature selection analysis of dataset

3 Machine learning models

3.1 Radial basis functions (RBF)

There are several functions that may be utilized as the RBF [26], [27], [28].

$$\varphi(r) = e^{-\frac{r^2}{2\sigma^2}}, \quad Gaussian \tag{1}$$

$$\varphi(r) = \frac{1}{(\sigma^2 + r^2)^{\alpha}}, \quad \alpha > 0, \tag{2}$$

$$\varphi(r) = (\sigma^2 + r^2)^{\beta}, \quad 0 < \beta < 1, \tag{3}$$

$$\varphi(r) = r, \quad liner, \tag{4}$$

$$\varphi(r) = r^2 In(r), \quad thin\ plate\ spline, \tag{5}$$

$$\varphi(r) = \frac{1}{1 + e^{\left(\frac{r}{\sigma^2}\right) - \theta}}, \quad logestic\ function, \tag{6}$$

where σ in Eqs (1), (2), (3), and (6) controls the interpolating function's smoothness, θ in Eq. (6) is an adjustable bias, and $r > 0$ indicates the distance between a data point $\vec{x}$ and a center c. The RBF transforms into Hardy's multiquadric function, which is widely employed in surface interpolation with excellent results, when β in Eq. (3) has the value of $\frac{1}{2}$. $\emptyset r$ is appropriate for DSP implementation when α in Eq. (2) is unity [29].

Localized RBFs with the characteristic that $\emptyset r \to 0$ as $r \to \infty$ are among these RBFs; they are Eqs (1), (2), and (6). Physiologically, cortical cells have receptive fields that resemble Gaussian curves. For this reason, the RBF is usually used as the Gaussian. The Gaussian has a positive density. It is driven by the principles of kernel density estimation and kernel regression. The Gaussian is the best basis function in the least-squares (LS) sense [30] for fitting data with normally distributed noise in the inputs. The only factorizable RBF is the Gaussian, which is a desired feature for the RBF network's hardware implementation.

Selected from a curve-fitting standpoint [31], the thin-plate spline function (Eq. 5) is a popular Radial Basis Function (RBF) for universal approximation. When fitting a surface based on a set of points and incorporating a roughness penalty [32], the thin-plate spline provides the solution. Over the range of $r \in (0, 1)$, it is negative and diverges at infinity. However, the estimated function must only be defined within a predetermined range for training purposes. A little amount of empirical data indicates that in high-dimensional environments, the thin-plate spline provides a superior fit to the data.

By choosing the standard deviation σ in the Gaussian Eq. (1) as two distinct positive values, σ_- for $x < 0$ and σ_+ for $x > 0$ [33], a pseudo-Gaussian function is introduced in the one-dimensional space. The pseudo-Gaussian function in each dimension is multiplied to extend this function to the multiple-dimensional space. Because of its radial asymmetry, the pseudo-Gaussian function is not technically an RBF; yet, this gives the hidden units more freedom in terms of function approximation [34].

It is most challenging and inefficient to use localized RBFs to approximate functions with segments that have values that are almost constant. This issue may be resolved by using the sigmoidal RBF, which is a composite of a collection of sigmoidal functions [35].

$$\varphi(r) = \frac{1}{1 + e^{-\beta[(x-c)+\theta]}} - \frac{1}{1 + e^{-\beta[(x-c)-\theta]}}, \tag{7}$$

Both θ and $\beta > 0$. The radial symmetry of $\varphi(x)$ reaches its greatest at c. The function's breadth is controlled by θ, while its steepness is controlled by β. If $\beta \times \theta$ is big, the form of $\varphi(x)$ is roughly rectangular, or more precisely, soft trapezoidal. For tiny β and θ, it has a bell-shaped form. By multiplying the appropriate function in each dimension, $\varphi(x)$ may be extended for the n-dimensional approximation. By including a compensatory term in the product term $\varphi_i(x_i)$, $\varphi(\vec{x})$ may be changed to allow for constant values of the intended output and prevent the kernel functions from being diminished [36]. Using the raised-cosine function as a one-dimensional RBF is another method. A constant function can be precisely represented by the raised-cosine RBF using two terms. It is possible to generalize this RBF to n dimensions [37]. By appropriately restricting certain parameters, various well-known fuzzy membership functions can accomplish the same goal [38].

The widely used Gaussian RBF has a circular form. To approximate a functional behavior with distinct noncircular properties, a large number of RBF nodes could be needed. A directed graph-based technique is used in [39] to incorporate direction-dependent scaling, shaping, and rotation of Gaussian RBFs for optimal trend sensing with minimal parameter representations for function approximation, therefore reducing the size of the RBF network.

3.2 Greylag goose optimization (GGO)

The study on environmental cleanup, and specifically noise reduction, shows how to effectively improve the BSS with GGO's assistance [40], [41], [42]. This section outlines the full suggestion on how GGO may optimize LSTM hyperparameters and adjust BSS settings.

3.2.1 GGO algorithm

The first step of the GGO algorithm is to create individuals who come up with potential solutions to the problem at random. These potential answers are represented by each individual. The population of the group, n, is represented by the term GGO $(X_i, i = 1,2, \ldots, n)$, where an integer represents the population's size [43], [44].

This illustration perfectly conveys how GGO moves through the solution space, finding a balance between exploitation (improving existing solutions) and exploration (looking for new, maybe better ones). The dynamic depiction of GGO's iterative process in the image highlights how the algorithm combines exploration and exploitation tactics in the best possible way to provide effective and efficient solutions [45].

3.2.2 Exploration operation

The GGO algorithm's exploration process is crucial; it involves searching the search space for the likely best solution, which causes GGO to steer toward the global optima and avoid local optima [46].

Getting to the Best Answer: This tactic lowers the likelihood of becoming locked in local optimality by using explorers' geese, who actively seek out excellent spots close to the ones that are already there. During iterations, the GGO method uses the following equations to update vectors A and C, which are represented as $A = 2a \cdot r_1 - a$ and $C = 2.r_2$, respectively. From 2 to 0, the parameter a change linearly:

$$X(t+1) = X^*(t) - A \cdot |C.X^*(t) - X(t)| \quad (8)$$

In this case, r_1 and r_2 are randomly fluctuating values inside [0,1], $X(t)$ indicates the position of an agent at iteration t, and $X^*(t)$ indicates the position of the best solution (leader).

The method uses the following formula to improve exploration even further, taking into account three randomly selected search agents (paddings), represented by the symbols $X_{"Paddle"1}$, $X_{"Paddle"2}$, and $X_{"Paddle"3}$:

$$\begin{aligned} X(t+1) = {} & w_1 X_{"Paddle"1} \\ & + zw_2(X_{"Paddle"2} \\ & - X_{"Paddle"3}) \\ & + (1-z)w_3(X \\ & - X_{"Paddle"1}) \end{aligned} \quad (9)$$

In this case, z drops exponentially in accordance with $z = 1 - (\frac{t}{t_{max}})^2$, where t is the number of iterations and tmax is the maximum number of iterations, whereas w_1, w_2, and w_3 update inside [0,2].

The values of a and vector A are decreased when $r_3 > 0.5$ in the second updating procedure:

$$\begin{aligned} X(t+1) = {} & w_4|X^*(t) \\ & - X(t)|e^{b\ell}\cos(2\pi\ell) \\ & + 2w_1(r_4 + r_5)X^*(t) \end{aligned} \quad (10)$$

Here, w_4 updates within [0,2], r_4 and r_5 update within [0,1], b is a constant, and ℓ is a random number in $[-1,1]$.

3.2.3 Exploitation operation

The exploitative component of the GGO algorithm focuses on refining previously found solutions. After each cycle, GGO identifies the entity with the highest fitness and assigns it the appropriate credit. Two distinct strategies, outlined below, are used to achieve the exploitation goals, and they work together to enhance the overall solution quality.

Getting to the Best Answer: Under the direction of three sentry solutions ($X_{"Sentry1"}$, $X_{"Sentry2"}$, and $X_{"Sentry3"}$), the algorithm uses the following equation to direct people ($X_{"NonSentry"}$) toward the predicted position of the prey:

$$\begin{aligned} X_1 &= X_{"Sentry1"} - A_1 \cdot |C_1 \cdot X_{"Sentry1"} - X|, \\ X_2 &= X_{"Sentry2"} - A_2 \cdot |C_1 \cdot X_{"Sentry2"} - X|, \\ X_3 &= X_{"Sentry3"} - A_3 \cdot |C_1 \cdot X_{"Sentry3"} - X|, \end{aligned} \quad (11)$$

where C_1, C_2, and C_3 are calculated as $C = 2r_2$, and A_1, A_2, and A_3 are calculated as $A = 2a \cdot r_1 - a$. The average of the three solutions, X_1, X_2, and X_3, is used to represent the updated locations for the population, $X(t+1)$, as follows:

$$X(t+1) = 1/3 \sum_{i=1}^{3} X_i \quad (12)$$

3.2.4 Searching the area around the best solution

In the pursuit of enhancements, individuals explore regions proximate to the optimal response (leader), denoted as $X_{"Flock"1}$. This exploration process is formulated by the equation:

$$\begin{aligned} X(t+1) = {} & X(t) \\ & + D(1+z)w(X \\ & - X_{"Flock"1}) \end{aligned} \quad (13)$$

In this case, D, z, and w all contribute to the exploration process, with z being determined by $z = 1 - (\frac{t}{tmax})^2$, where t is the number of iterations and tmax is the maximum number of iterations.

3.3 Leader Harris Hawks optimization (LHHO)

The development of the leader Harris hawks optimization (LHHO) was motivated by the inquisitive behavior of the Harris hawk. The limited exploring capabilities of the HHO are one of its disadvantages. The cause is the perching strategy, which depends on equal chance q. The HHO method [47] states that if $q < 0.5$, the hawks perch based on where other family members are; if $q > 0.5$, they perch randomly on a tall tree. The chance of a perch for a single hawk can assist circumvent this.

Exploration phase ($|E| \geq 1$): Using the current hawk's fitness value with position vector X_i as $f(X_i)$ of ith hawk, the best-performing hawk's position vector X_{prey} as $f(X_{prey})$, and the worst-performing hawk's position vector X_{worst} as $f(X_{worst})$, we can define an adaptive perch probability (p_{ap}^i) of the ith hawk. Next, the following model may be used to express the adaptive perch probability (p_{ap}^i):

$$p_{ap}^i = \frac{|f(X_i) - f(X_{prey})|}{|f(X_{worst}) - f(X_{prey})|}, i = 1, 2, \ldots, N. \quad (14)$$

The inquiry phase may thus be shown as

$$X_i(new) = \begin{cases} X_{rand}(t) - r_1|X_{rand}(t) - 2r_2X_i(t)|, & q \geq p_{ap}^i \\ \left(X_{prey}(t) - X_m(t)\right) - r_3\left(LB + r_4(UB - LB)\right), & q < p_{ap}^i \end{cases}. \quad (15)$$

where $X_m(t)$ represents the mean location vector of the N hawk population at any given time. Phase of exploitation ($|E| < 1$): The exploitation phase can be imitated using the four possible attacking strategies that are comparable to the HHO and are described below [47], [48].

- *Soft besiege, in which $r \geq 0.5$ and $|E| > 0.5$.*

$$X_i(new) = X_{prey}(t) - X_i(t) - E\left|JX_{prey}(t) - X_i(t)\right|. \quad (16)$$

where J is the jump strength as determined by Eq. (16).

- *Hard besiege, in which $r > 0.5$ and $|E| < 0.5$.*

$$X_i(new) = X_{prey}(t) - E\left|X_{prey}(t) - X_i(t)\right|. \quad (17)$$

- *Gradual fast dives with soft besiege ($r < 0.5$ and $|E| \geq 0.5$).*

$$X_i(new) = \begin{cases} Y_i & if\ f(Y_i) < f\left(X_i(t)\right) \\ Z_i & if\ f(Z_i) < f\left(X_i(t)\right) \end{cases}. \quad (18)$$

- *intense barrage with progressively faster dives ($r < 0.5$ and $|E| < 0.5$).*

$$X_i(new) = \begin{cases} Y_i & if\ f(Y_i) < f\left(X_i(t)\right) \\ Z_i & if\ f(Z_i) < f\left(X_i(t)\right) \end{cases}. \quad (19)$$

The HHO algorithm's exploration phase transitions to exploitation based on the prey's escape energy [49].

Leader-dependent mutation selection Let's determine the best position vector ($X^{\,t}_{best}$), second-best ($X^{\,t}_{best-1}$), and third-best ($X^{\,t}_{best-2}$) among N individual hawks. Adjust position vectors according to the new position vector $X(new)$'s fitness function value. Thus, $X_i(mut)$, the new mutation location vector for the ith bird, may be explained as follows:

$$X_i(mut) = X_i(new) + 2 \times \left(1 - \frac{t}{t_{max}}\right) \times (2 \times rand - 1)(2 \times X_{best}^t(X_{best-1}^t + X_{best-2}^t)) + (2 \times rand - 1)(X_{best}^t - X_i(new)). \quad (20)$$

where $rand$ is a random number that falls between 0 and 1.

The location vector for the subsequent generation $X_i(t+1)$ may then be obtained by applying the selection process described in Eq. (21). Similarly, the X_{prey} is updated using Eq. (22).

$$X_i(t+1) = \begin{cases} X_i(mut) & f\left(X_i(mut)\right) < f\left(X_i(new)\right) \\ X_i(new) & f\left(X_i(mut)\right) \geq f\left(X_i(new)\right) \end{cases}. \quad (21)$$

$$X_{prey} = \begin{cases} X_i(mut) & f\left(X_i(mut)\right) < f\left(X_{prey}\right) \\ X_i(new) & f\left(X_i(new)\right) < f\left(X_{prey}\right) \end{cases}. \quad (22)$$

3.4 Performance evaluators

- ***Root Mean Square Error (RMSE):*** RMSE measures the average size of the error between expected and actual values. It provides an overall indication of how well a model fits the data: the lower the RMSE, the better the model's predictions. By squaring the errors, RMSE gives greater weight to larger discrepancies.

$$RMSE = \sqrt{\frac{1}{n}\sum_{i=1}^{n}(O_i - P_i)^2} \quad (23)$$

- ***R-squared (R^2):*** The quality of fit, or how closely the model's predictions match the real data, is explained by R^2. It indicates the extent to which the model accounts for the variation. An excellent match is indicated by a value near 1, whereas a value around 0 indicates a limited predictive capacity.

$$R^2 = 1 - \frac{\sum_{i=1}^{n}(O_i - P_i)^2}{\sum_{i=1}^{n}(O_i - \bar{P}_i)^2} \quad (24)$$

- ***Mean Squared Error (MSE):*** The average squared difference between forecasts and actuals is determined by the MSE. Larger mistakes are highlighted due to the squaring, which makes it helpful for evaluating regressions where a lower value denotes better performance.

$$MSE = \frac{1}{n}\sum_{i=1}^{n}(O_i - P_i)^2 \quad (25)$$

- ***Weighted Absolute Percentage Error (WAPE):*** WAPE is a statistic used to assess a forecast's accuracy. It refers to the ratio of the sum of the actual values to the total absolute error. The lower WAPE, the better. Additionally, it is less susceptible to outliers than, say, RMSE or MSE.

$$WAPE = \frac{\sum_{i=1}^{n}\left|O_{i_i} - P_i\right|}{\sum_{i=1}^{n}|O_i|} \times 100 \quad (26)$$

- ***Nash-Sutcliffe Efficiency (NSE):*** NSE compares a model's prediction ability to the average of the observed data. The values vary from 1.0, which denotes perfect coincidence of anticipated and actual values, to negative values, which indicate bad forecasts. Poor prediction performance is shown by values close to 0.

$$NSE = 1 - \frac{\sum_{i=1}^{n}(O_i - P_i)^2}{\sum_{i=1}^{n}(O_i - \bar{O})^2} \quad (27)$$

where:
O_i = observed values,
P_i = predicted values,
$\bar{O}$ = mean of observed values,
n = number of observations.

3.5 Hyperparameter tuning

The hyperparameter tuning outcomes for the three predictive models, RBF+GGO (RBGG), RBF+LHHO (RBLH), and RBF, used in this investigation are compiled in Table 2. Since hyperparameter tuning directly affects the model's capacity to identify intricate patterns in the data, it is an essential step in maximizing model performance. The spread and the number of centers (Num_centers) are the two main hyperparameters taken into account. These two factors are crucial in determining the architecture and generalization potential of the RBF network. With 20 centers and a spread of 0.3, the RBGG model performed at its best, suggesting that a larger network is preferred in order to capture intricate interactions. Despite requiring a wider spread (0.6) but slightly fewer centers (18), the RBLH model appears to benefit from a smoother function approximation. On the other hand, due to its simpler architecture, the base RBF model performed best with just 10 centers and a spread of 0.5. These setups guarantee that every model is optimized for precision, dependability, and computational effectiveness.

The standalone RBF model required approximately 2 minutes to train, while the hybrid RBGG and RBLH models needed around 8 and 11 minutes, respectively, on a system equipped with 16 GB RAM and an Intel Core i7-1165G7 processor (2.80 GHz). The additional runtime for the hybrid models is due to the iterative nature of the optimization algorithms, which balance computational cost with improved predictive performance.

All data preprocessing, model development, optimization, and visualization tasks were performed using Python. Core libraries included NumPy and Pandas for data handling, Scikit-learn for machine learning implementation, and Matplotlib and Seaborn for plotting and visualization.

Table 2: The result of the hyperparameter

Models	Hyperparameter	
	Num_centers	Spread
RBGG	20	0.3
RBLH	18	0.6
RBF	10	0.5

4 Results

Table 3 compares three predictive models RBGG, RBLH, and RBF across the training, validation, and testing phases, using key performance metrics such as RMSE, R^2, MSE, WAPE, and NSE. Evaluating these models will help identify the most accurate and reliable model for predicting pile capacity, a critical factor in geotechnical engineering projects.

In the training phase of the RBGG model, the predictive performance was strong, with an RMSE value of 335.915 and a high R^2 value of 0.957. This indicates that the model explains 95.7% of the variance in pile capacity based on input features including geotechnical properties (such as average cohesion, average friction, and average soil specific weight) and geometric characteristics (such as pile area). These distinct feature categories collectively influence the model's ability to predict axial bearing capacity. However, validation and testing phases showed a decline in performance. RMSE increased to 392.524 and 427.938 for validation and testing, respectively, while R^2 dropped to 0.931 during testing. Additionally, the WAPE rose to 0.136 in testing, and the NSE deteriorated to 0.910, suggesting that the model has less ability to generalize and may be overfitting with new data.

In contrast, the RBLH model shows a different trend, performing well across all phases with a consistent RMSE reduction from training to validation and testing: 293.570, 343.919, and 368.305, respectively. The R^2 values reflect strong predictive accuracy, especially with a high-test score of 0.961. This suggests that the RBLH model is stable in its predictions, likely due to its ability to effectively utilize relationships between input variables such as average pile-soil friction and pile length, which are crucial for determining pile performance. While WAPE and MSE slightly increased during validation and testing, the NSE values remain relatively high at 0.931, indicating that the RBLH model offers reliable generalization on unseen data.

The RBF model outperforms both the RBGG and RBLH models across all phases. In the training phase, an RMSE value of 183.680 with an R^2 of 0.986 indicates that the model effectively captures complex interactions among input variables, particularly flap number and pile area, which are essential for accurately estimating pile capacity. During the validation phase, the RBF model still shows low prediction errors, with an RMSE of 214.325 and an R^2 of 0.980, demonstrating its strong generalizability. Further confirmation of the model's strength comes from the testing phase, where it achieves an RMSE of 224.246, a low MSE of 5.03E+04, and a competitive NSE of 0.873. While performance is slightly lower during testing, the model still demonstrates strong predictive capabilities, indicating its efficiency in handling the complexity of geotechnical data.

In summary, the RBF model has shown the best performance in the estimation of Pile Capacity with minimum errors and maximum accuracy during all phases. The strong results can be attributed to the model's ability to effectively make use of the input features, which were representatives of critical geotechnical factors such as soil properties, pile dimensions, and load-bearing characteristics. The RBLH model follows closely, showing stable and reliable predictions, while the RBGG model has some overfitting issues that question its generalizability. These findings bring to light the importance of choosing robust predictive models, such as RBF for Pile Capacity estimation, toward the optimization of design for ensuring structural safety in geotechnical engineering projects.

In contrast, the RBLH model consistently outperformed both RBF and RBGG in terms of R^2 and RMSE on both training and testing datasets, demonstrating high accuracy and robustness. The RBGG model, although slightly less accurate than RBLH in some instances, exhibited stable generalization behavior,

particularly when tested under varied soil and pile conditions. This suggests that while RBLH is the overall best-performing model, RBGG may be preferable in scenarios where robustness across diverse inputs is a priority.

Therefore, RBLH is identified as the most accurate and reliable model for predicting pile bearing capacity in this study, whereas RBGG offers valuable generalization potential under fluctuating conditions.

Table 3: The outcome of the constructed models for RBF

Model	Phase	Index values				
		RMSE	R^2	MSE	WAPE	NSE
RBGG	Train	335.915	0.957	1.13E+05	0.103	0.945
	Validation	392.524	0.942	1.54E+05	0.120	0.925
	Test	427.938	0.931	1.83E+05	0.136	0.910
RBLH	Train	293.570	0.950	8.62E+04	0.144	0.937
	Validation	343.919	0.932	1.18E+05	0.170	0.914
	Test	368.305	0.961	1.36E+05	0.165	0.931
RBF	Train	183.680	0.986	3.37E+04	0.083	0.974
	Validation	214.325	0.980	4.59E+04	0.096	0.964
	Test	224.246	0.923	5.03E+04	0.107	0.873

Fig. 3 shows the convergence trace for two hybrid models, RBGG and RBLH, during the training process, along with their respective Root Mean Square Error (RMSE) values. Both models start with the same initial RMSE of 585, indicating they begin at the same level of predictive accuracy. However, during the first 70 iterations, the RBGG model exhibited higher RMSE values compared to RBLH, suggesting initial instability or slower adaptation to the data. As the iterations progressed, RBGG showed substantial improvement, demonstrating a strong convergence path. By the end of the optimization process, the RBGG model significantly outperformed RBLH, achieving an RMSE value 56.61 times lower, with a final RMSE score of 392.52. This result highlights the superior learning capability and optimization efficiency of the RBGG model, making it more suitable for enhancing the predictive accuracy of pile capacity in geotechnical applications.

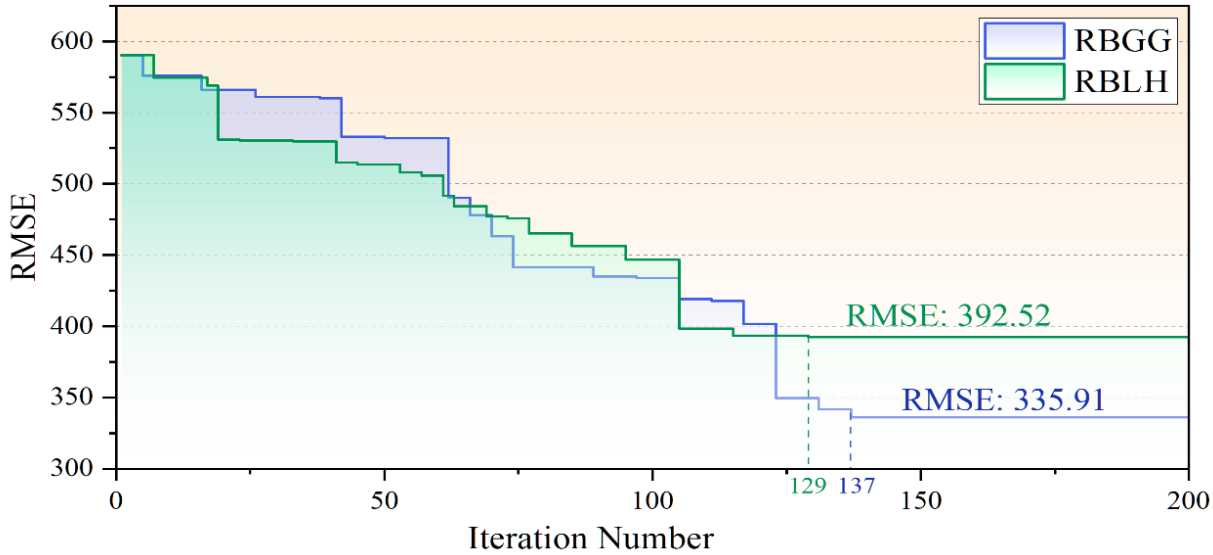

Figure 3: The convergence curves of the two hybrid models being showcased

The dispersion graphs of the hybrid models that evolved are shown in Fig. 4, together with the performances regarding RMSE and R^2 scores for the Train, Validation, and Test phases. This graph is needed to deeply understand how each model performs with respect to the ideal Best Fit line. Among the model comparison presented, RBGG proved to be more consistent, where results are well-clustered in a tight range of $[-10\%x, 10\%x]$, depicting very strong predictive accuracy in each phase. On the other hand, the base model RBF yielded more scattered results from the Best Fit line, indicating greater variability and lower reliability of that model's predictions. These patterns highlight how developments made using the RBGG model minimized errors and increased correlation, thus providing close agreement with the focus of this study on the optimization of hybrid models to enhance pile capacity prediction accuracy.

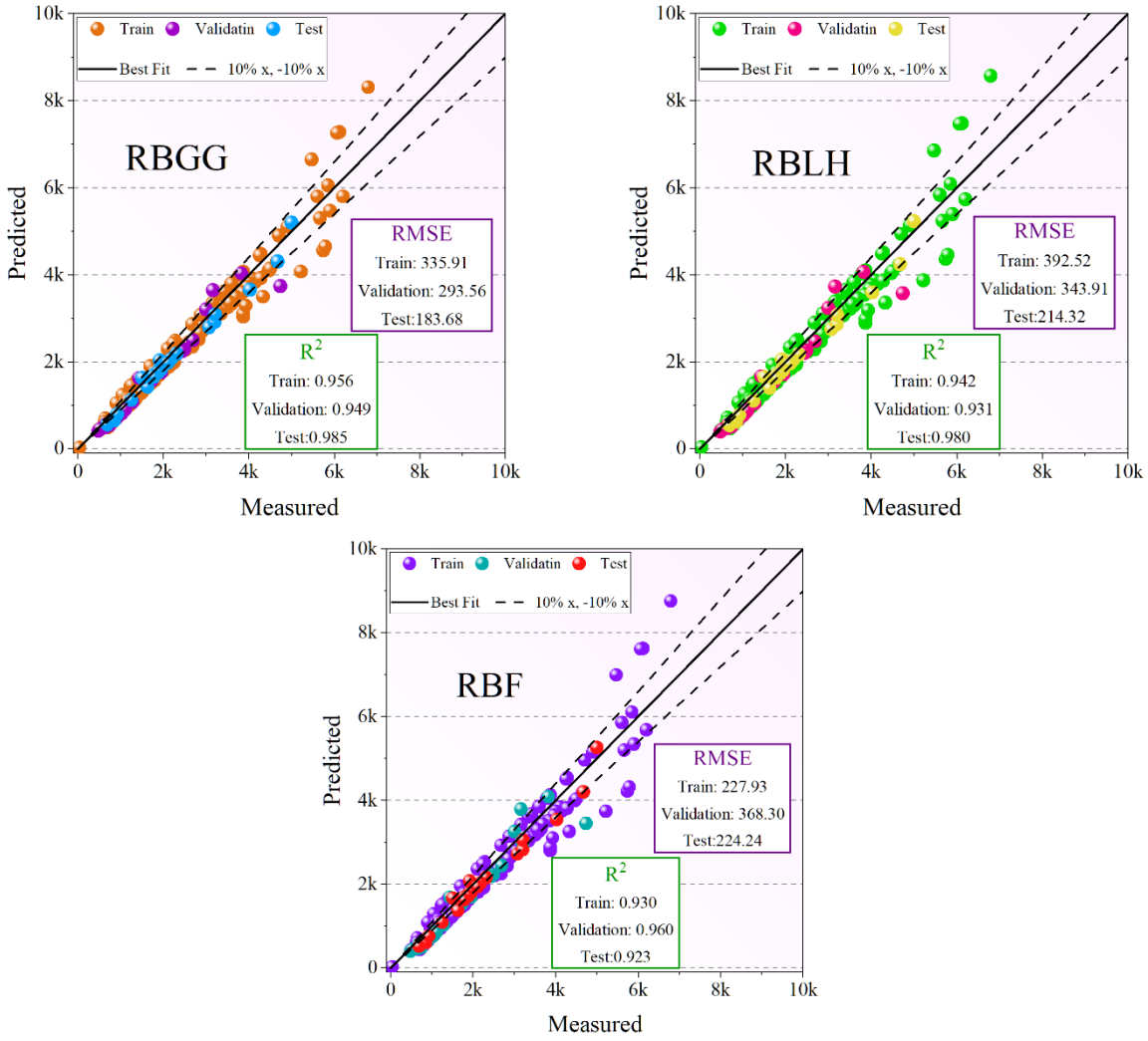

Figure 4: The dispersion of evolved hybrid models

Fig. 5 provides a detailed comparison between the predictions of the hybrid models and the actual observed data, emphasizing the predictive accuracy of each model. The RBGG model consistently outperforms the others across all three important phases: Training, Validation, and Testing. It demonstrates an impressive match with the actual values, with deviations being minimal compared to the other models. This indicates that RBGG is the most reliable model for generalization across different datasets. By making predictions that closely align with the measured data, the RBGG model stands out as the most dependable among those studied. As a result, it is particularly suitable for applications requiring high precision in predicting pile capacity and related geotechnical parameters. The consistency of RBGG in delivering accurate predictions reinforces its practical value, especially in optimizing pile design and ensuring structural safety in engineering projects.

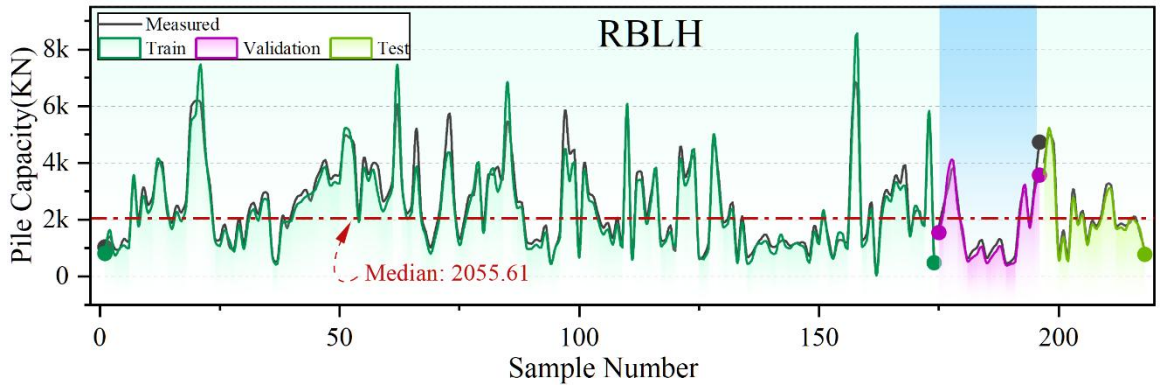

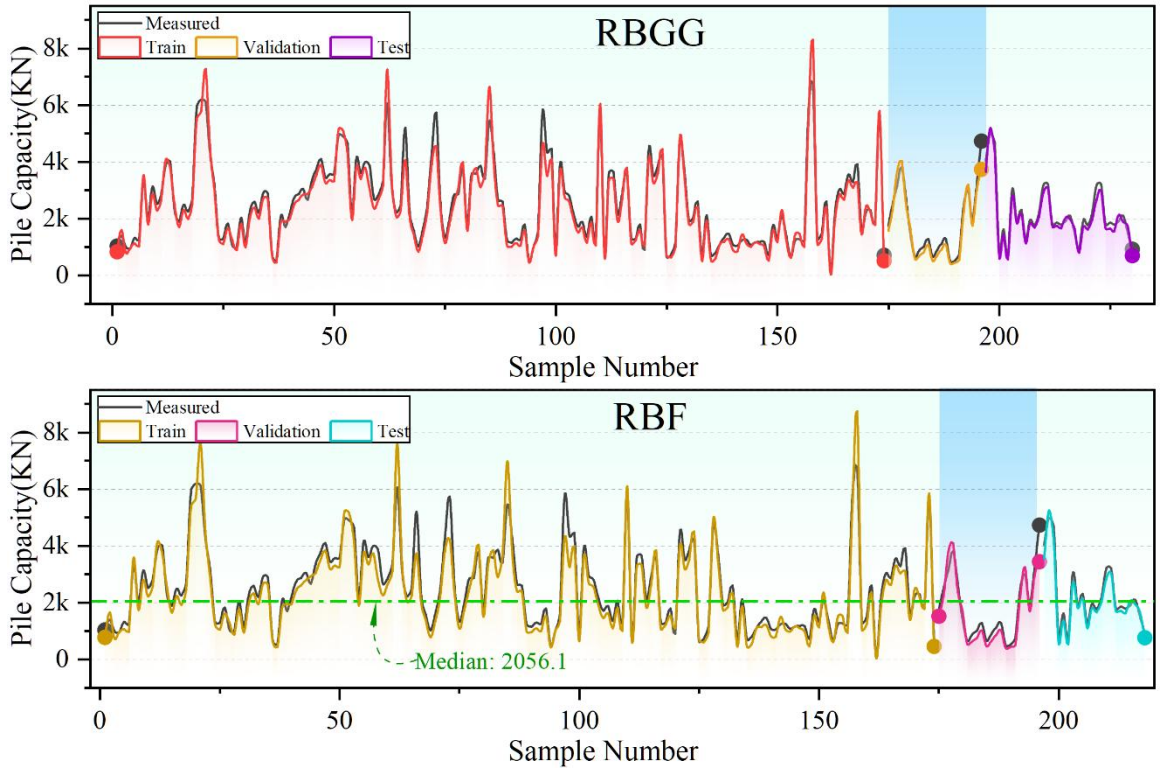

Figure 5: The comparison between forecasted and actual values

Fig. 6 illustrates the error percentages of the RBF, RBLH, and RBGG models using a vertical bar plot across the Training, Validation, and Testing phases. The enhanced figure includes labeled axes for error percentage, consistent color coding for each model, and a comprehensive legend. The RBGG model exhibits the most constrained error range, from -28.571% to 22.404%, suggesting high accuracy and low variance. This narrow span reflects the model's robustness and adaptability, particularly under varying data conditions. Despite its overall superior performance, a few mild outliers can be observed in the RBGG model, primarily during the training phase. These may be attributed to inherent noise or measurement uncertainties in the input dataset rather than model instability. Importantly, these outliers do not significantly impact the model's overall predictive performance, as evidenced by its consistent results in the validation and testing phases.

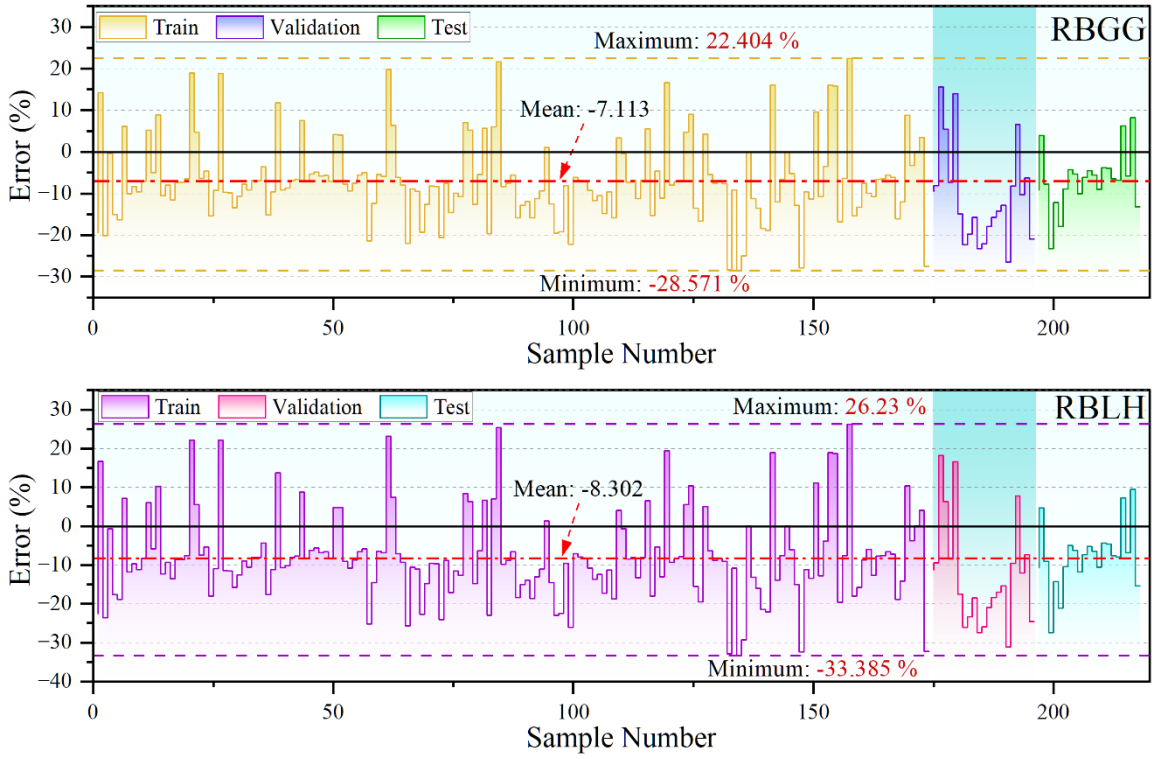

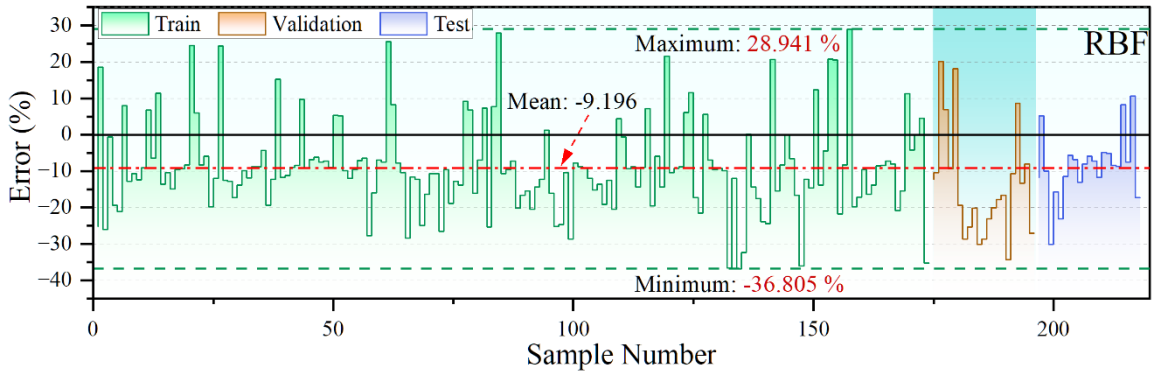

Figure 6: The error percentage of the models is derived from the vertical plot

Fig. 7 presents a raincloud plot to provide a comprehensive view of the error distribution across all three phases. This visualization combines density curves, box plots, and raw data scatter, offering insights into spread and skewness. RBGG again demonstrates the tightest distribution and lowest error spread (Train: -7%, Validation: -11%, Test: -6%). The minimal presence of long tails or extreme values supports the model's precision and generalization capability. Collectively, the updated visualizations and expanded discussion reinforce the strength of the RBGG model not only in average accuracy but also in error consistency and resilience to outlier effects. This robustness is particularly valuable in practical geotechnical engineering applications, where prediction reliability under uncertainty is critical.

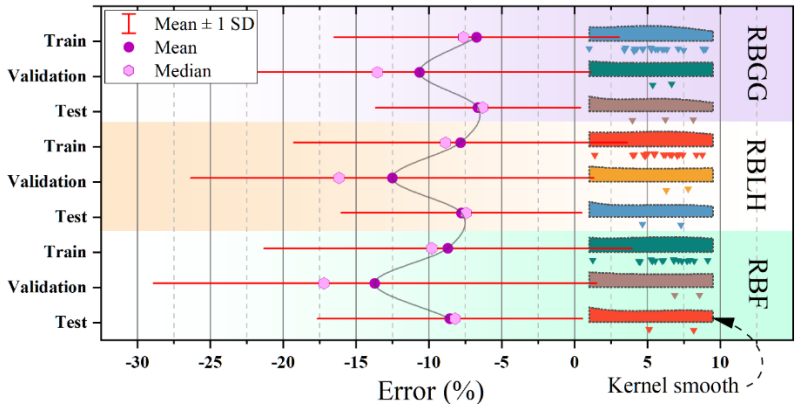

Figure 7: The error raincloud plot of the proposed models

The SHAP (SHapley Additive exPlanations) values that are used to assess each input feature's relative contribution to pile capacity prediction are shown in Fig. 8. By giving each feature an importance value determined by how much it contributes to the model's prediction, SHAP analysis is a potent interpretability technique that clarifies the results of machine learning models. Pile Capacity has the highest SHAP value in this figure, confirming its direct function as the output target. The most important characteristics among the input variables are Pile Length, Average Friction Angle, and Flap Number; each makes a substantial contribution to the prediction model. These factors are essential for capturing the mechanical, depth, and resistance effects of soil conditions on pile performance. Both average soil specific weight and average pile-soil friction angle show a moderate amount of influence, suggesting that they play a part in determining the characteristics of effective stress and load transfer. Pile Area, on the other hand, exhibits little influence, indicating that its variation makes a smaller contribution to capacity prediction within the examined dataset. For more effective, precise, and understandable pile capacity prediction techniques in practical engineering applications, the SHAP analysis thus offers direct insights into which geotechnical parameters should be given priority during model development and optimization.

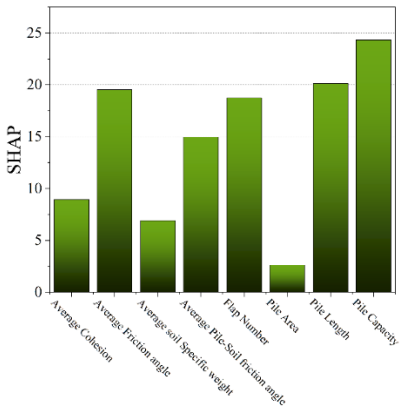

Figure 8: SHAP sensitivity analysis for feature impact evaluation

A comparative overview of the current study and earlier studies on pile capacity prediction using different modeling techniques is shown in Table 4. Regression and EPR-MOGA techniques were used by Alzabeebee et al. [19], who demonstrated how well EPR-MOGA captures nonlinear soil-friction interactions. For drilled shafts, Shahin [16] used ANN on 174 data points and obtained R^2 values as high as 0.97. Using important geotechnical inputs, Samui [17] employed SVM and achieved high, though unspecified, accuracy. M. Kumar et al. [20] used deep learning (e.g., XGBoost, RF) and ensemble methods, with XGBoost producing an R^2 of 0.91. Alzabeebee et al. [50] demonstrated in another study that EPR can predict undrained adhesion better than empirical models. When DNN and RNN variants were investigated by M. Kumar et al. [51], DNN performed the best (R^2 = 0.97). When Kumar et al. [52] combined ANN with different metaheuristics, GP and ANN-PSO achieved R^2 values greater than 0.97. Using 220 actual pile load test data, the current study presents a hybrid RBF-based model optimized with LHHO and GGO. The RBLH model, which included temporal factors, sensitivity analysis, and correlation-based input selection, had the highest accuracy (R^2 = 0.986), suggesting a significant contribution to predictive modeling in geotechnical engineering.

Table 4: Comparison between the presented and published studies

Study	Method Used	Dataset	Performance (R^2)	Highlights
[19]	Regression, EPR-MOGA	Not specified	EPR-MOGA: 0.85–0.92Regression: 0.16–0.67	EPR-MOGA captured complex soil-friction relationships in fine-grained soils
[16]	ANN	174 data points	0.85 (Driven piles)0.97 (Drilled shafts)	Effective for axial capacity prediction using ANN
[17]	SVM	Not specified	High accuracy (value not reported)	Used number of bowls, mean stress, and depth ratio as inputs
[20]	XGBoost, RF, GBM, DL	81 static load tests	XGBoost: 0.91	SHAP and Taylor diagrams used for model evaluation
[50]	EPR (Multi-objective)	Not specified	Superior to empirical methods	Predicted undrained adhesion factor in bored piles
[51]	DNN, CNN, RNN, LSTM, BiLSTM	257 dynamic load tests	DNN: 0.97	BiLSTM second best; RNN underperformed due to multicollinearity
[52]	ANN + PSO, GOA, ABC, ACO, ALOGP, MARS, GMDH	Dynamic pile load tests	ANN-PSO: 0.9773GP: 0.9859	Metaheuristic-optimized ANN superior to traditional models
Present Study	RBF + LHHO (RBLH), RBF + GGO (RBGG)	220, Real pile load test data	RBLH: R^2 = 0.986RMSE = 183.680	Novel hybrid model with time-dependent variables, correlation-based feature selection, high generalization, and sensitivity analysis

5 Conclusions

The key finding of this paper, in particular, highlights the central position of advanced predictive models to perform pile capacity estimations, the crucial element in geotechnical engineering. Key performance metrics, such as RMSE, R^2, MSE, WAPE, and NSE, were chosen for the evaluation of RBGG, RBLH, and RBF for the training, validation, and testing phases. It can be seen from the results that the best overall performance was given by the RBF model, with the minimum RMSE value and the highest R^2 value, especially in the training phase, which reflects its strong ability in capturing complex interactions of critical geotechnical variables, including soil properties and pile dimensions. However, this study also included a sensitivity analysis of time-varying features, which provided good insight into the behavior of models wrt

changes in dynamic factors over time. This sensitivity analysis continued to support the strength of the RBF model, given that at every instance it showed strong predictive performance, even when exposed to variations in input features across different phases. On the other hand, highly effective though the RBGG model was in training, it resulted in significant overfitting upon validation and testing, especially in decreasing performance with time-dependent variables introduced. It thus appears that RBGG fails to generalize over time, limiting its practical applicability.

The RBLH model, though not outcompeting RBF, showed consistent performance across all phases. Therefore, it proved to be a good choice for pile capacity prediction, especially when time-dependent factors were included. It gives solid performance with lower error margins and higher generalizability, pointing out its capacity to effectively incorporate the change of input features over time. In general, the results seem to underline the importance of precision and generalization in model selection for geotechnical applications. Among these, the performance of the RBF model is the most consistent and reliable due to its ability to adapt to time-dependent variables, thus it can be considered a very powerful tool in pile capacity estimation. Further studies can be done by incorporating more optimization techniques into the models for their strength and flexibility in adjusting to changing geotechnical conditions, which will be beneficial in enhancing prediction accuracy and reliability in real-world engineering projects.

Acknowledgements

I would like to take this opportunity to acknowledge that there are no individuals or organizations that require acknowledgment for their contributions to this work.

Competing of interests

The authors declare no competing of interests.

Authorship contribution statement

Shanwei Zhang: Writing-Original draft preparation, Conceptualization, Supervision, Project administration.

Data availability

On Request

Conflicts of interest

The authors declare that there is no conflict of interest regarding the publication of this paper.

Author statement

The manuscript has been read and approved by all the authors, the requirements for authorship, as stated earlier in this document, have been met, and each author believes that the manuscript represents honest work.

Funding

This research received no specific grant from any funding agency in the public, commercial, or not-for-profit sectors.

Ethical approval

All authors have been personally and actively involved in substantial work leading to the paper, and will take public responsibility for its content.

References

[1] K. Fakharian and M. Khanmohammadi, “Comparison of pile bearing capacity from CPT and dynamic load tests in clay considering soil setup,” *Frontiers in Offshore Geotechnics III; CRC Press: Boca Raton, FL, USA*, pp. 539–544, 2015.

[2] C. Su, L. Wang, Z. Wu, and H. Xu, “Research on weighing of concrete aggregate pile based on binocular vision,” *Informatica*, vol. 46, no. 7, 2022.

[3] B. Naeim, M. R. Akbarzadeh, and V. Jahangiri, “Machine learning-based prediction of seismic response of elevated steel tanks,” *Structures*, vol. 70, p. 107649, 2024, doi: https://doi.org/10.1016/j.istruc.2024.107649.

[4] M. Khanmohammadi and K. Fakharian, “Evaluation of performance of piled-raft foundations on soft clay: A case study,” *Geomechanics and Engineering*, vol. 14, no. 1, pp. 43–50, 2018.

[5] V. E. Komurka, A. B. Wagner, and T. B. Edil, “Estimating soil/pile set-up,” Citeseer, 2003.

[6] M. N. Haque and E. J. Steward, “Evaluation of pile setup phenomenon for driven piles in Alabama,” in *Geo-Congress 2020*, American Society of Civil Engineers Reston, VA, 2020, pp. 200–208.

[7] B. Naeim, A. J. Khiavi, P. Dolatimehr, and B. Sadaghat, “Novel Optimized Support Vector Regression Networks for Estimating Fresh and Hardened Characteristics of SCC,” 2024.

[8] E. Khajavi, A. R. Taghavi Khanghah, and A. Javadzade Khiavi, “An efficient prediction of punching shear strength in reinforced concrete slabs through boosting methods and metaheuristic algorithms,” *Structures*, vol. 74, p. 108519, 2025, doi: https://doi.org/10.1016/j.istruc.2025.108519.

[9] K. Fakharian and M. Khanmohammadi, “Effect of OCR and pile diameter on load movement response of piles embedded in clay over time,” *International Journal of Geomechanics*, vol. 22, no. 7, p. 4022091, 2022.

[10] R. Skov and H. Denver, “Time-dependence of bearing capacity of piles,” in *Proc. Third International Conference on the Application of Stress-Wave Theory to Piles. Ottawa*, 1988, pp. 25–27.

[11] M. W. Gardner and S. R. Dorling, “Artificial neural networks (the multilayer perceptron)—a review of applications in the atmospheric sciences,” *Atmos Environ*, vol. 32, no. 14–15, pp. 2627–2636, 1998.

[12] M. Parsajoo, D. J. Armaghani, A. S. Mohammed, M. Khari, and S. Jahandari, “Tensile strength prediction

of rock material using non-destructive tests: A comparative intelligent study," *Transportation Geotechnics*, vol. 31, p. 100652, 2021.

[13] D. Li, Z. Liu, D. J. Armaghani, P. Xiao, and J. Zhou, "Novel ensemble tree solution for rockburst prediction using deep forest," *Mathematics*, vol. 10, no. 5, p. 787, 2022.

[14] M. Koopialipoor, P. G. Asteris, A. S. Mohammed, D. E. Alexakis, A. Mamou, and D. J. Armaghani, "Introducing stacking machine learning approaches for the prediction of rock deformation," *Transportation Geotechnics*, vol. 34, p. 100756, 2022.

[15] I.-M. Lee and J.-H. Lee, "Prediction of pile bearing capacity using artificial neural networks," *Comput Geotech*, vol. 18, no. 3, pp. 189–200, 1996.

[16] M. A. Shahin, "Intelligent computing for modeling axial capacity of pile foundations," *Canadian Geotechnical Journal*, vol. 47, no. 2, pp. 230–243, 2010.

[17] P. Samui, "Prediction of pile bearing capacity using support vector machine," *International Journal of Geotechnical Engineering*, vol. 5, no. 1, pp. 95–102, 2011.

[18] E. Momeni, R. Nazir, D. J. Armaghani, and H. Maizir, "Prediction of pile bearing capacity using a hybrid genetic algorithm-based ANN," *Measurement*, vol. 57, pp. 122–131, 2014.

[19] S. Alzabeebee, B. Ismael, S. Keawsawasvong, and A. W. Alshami, "Evolutionary Polynomial Regression Model to Predict Effective Angle of Internal Friction of Fine-Grained Soils," *Transportation Infrastructure Geotechnology*, vol. 12, no. 2, p. 97, 2025, doi: 10.1007/s40515-025-00557-0.

[20] M. Kumar, S. Pijush, K. Divesh Ranjan, and P. G. and Asteris, "State-of-the-art XGBoost, RF and DNN based soft-computing models for PGPN piles," *Geomechanics and Geoengineering*, vol. 19, no. 6, pp. 975–990, Nov. 2024, doi: 10.1080/17486025.2024.2337702.

[21] F. Milad, T. Kamal, H. Nader, and O. E. Erman, "New method for predicting the ultimate bearing capacity of driven piles by using Flap number," *KSCE Journal of Civil Engineering*, vol. 19, no. 3, pp. 611–620, Mar. 2015, doi: 10.1007/s12205-013-0315-z.

[22] D. Jahed Armaghani, R. S. N. S. B. R. Shoib, K. Faizi, and A. S. A. Rashid, "Developing a hybrid PSO–ANN model for estimating the ultimate bearing capacity of rock-socketed piles," *Neural Comput Appl*, vol. 28, no. 2, pp. 391–405, Feb. 2017, doi: 10.1007/s00521-015-2072-z.

[23] S. Shaik, K. S. R. Krishna, M. Abbas, M. Ahmed, and D. Mavaluru, "Applying several soft computing techniques for prediction of bearing capacity of driven piles," *Eng Comput*, vol. 35, no. 4, pp. 1463–1474, Oct. 2019, doi: 10.1007/s00366-018-0674-7.

[24] A. Dehghanbanadaki, M. Khari, S. T. Amiri, and D. J. Armaghani, "Estimation of ultimate bearing capacity of driven piles in c-φ soil using MLP-GWO and ANFIS-GWO models: a comparative study," *Soft comput*, vol. 25, no. 5, pp. 4103–4119, Mar. 2021, doi: 10.1007/s00500-020-05435-0.

[25] H. Harandizadeh, D. Jahed Armaghani, and M. Khari, "A new development of ANFIS–GMDH optimized by PSO to predict pile bearing capacity based on experimental datasets," *Eng Comput*, vol. 37, no. 1, pp. 685–700, Jan. 2021, doi: 10.1007/s00366-019-00849-3.

[26] T. Poggio and F. Girosi, "Networks for approximation and learning," *Proceedings of the IEEE*, vol. 78, no. 9, pp. 1481–1497, 1990.

[27] C. A. Micchelli, *Interpolation of scattered data: distance matrices and conditionally positive definite functions*. Springer, 1984.

[28] Y. Liao, S.-C. Fang, and H. L. W. Nuttle, "Relaxed conditions for radial-basis function networks to be universal approximators," *Neural Networks*, vol. 16, no. 7, pp. 1019–1028, 2003.

[29] K.-L. Du, K. K. M. Cheng, and M. N. S. Swamy, "A fast neural beamformer for antenna arrays," in *2002 IEEE International Conference on Communications. Conference Proceedings. ICC 2002 (Cat. No. 02CH37333)*, IEEE, 2002, pp. 139–144.

[30] A. R. Webb, "Functional approximation by feed-forward networks: a least-squares approach to generalization," *IEEE Trans Neural Netw*, vol. 5, no. 3, pp. 363–371, 1994.

[31] D. Lowe, "On the use of nonlocal and non positive definite basis functions in radial basis function networks," 1995.

[32] J. Meinguet, "Multivariate interpolation at arbitrary points made simple," *Zeitschrift für angewandte Mathematik und Physik ZAMP*, vol. 30, no. 2, pp. 292–304, 1979.

[33] I. Rojas *et al.*, "Time series analysis using normalized PG-RBF network with regression weights," *Neurocomputing*, vol. 42, no. 1–4, pp. 267–285, 2002.

[34] C.-J. Lin and W.-H. Ho, "A pseudo-Gaussian-based compensatory neural fuzzy system," in *The 12th IEEE International Conference on Fuzzy Systems, 2003. FUZZ'03.*, IEEE, 2003, pp. 214–219.

[35] C.-C. Lee, P.-C. Chung, J.-R. Tsai, and C.-I. Chang, "Robust radial basis function neural networks," *IEEE Transactions on Systems, Man, and Cybernetics, Part B (Cybernetics)*, vol. 29, no. 6, pp. 674–685, 1999.

[36] S.-J. Lee and C.-L. Hou, "An ART-based construction of RBF networks," *IEEE Trans Neural Netw*, vol. 13, no. 6, pp. 1308–1321, 2002.

[37] R. J. Schilling, J. J. Carroll, and A. F. Al-Ajlouni, "Approximation of nonlinear systems with radial basis function neural networks," *IEEE Trans Neural Netw*, vol. 12, no. 1, pp. 1–15, 2001.

[38] K.-L. Du and M. N. S. Swamy, *Neural networks in a softcomputing framework*, vol. 501. Springer, 2006.

[39] P. Singla, K. Subbarao, and J. L. Junkins, "Direction-dependent learning approach for radial basis function networks," *IEEE Trans Neural Netw*, vol. 18, no. 1, pp. 203–222, 2007.

[40] G. Szipl, A. Loth, C. A. F. Wascher, J. Hemetsberger, K. Kotrschal, and D. Frigerio, "Parental behaviour and family proximity as key to gosling survival in Greylag Geese (Anser anser)," *J Ornithol*, vol. 160, pp. 473–483, 2019.

[41] M. Hoarau, F. Angelier, F. Touzalin, T. Zgirski, C. Parenteau, and P. Legagneux, "Corticosterone: foraging and fattening puppet master in pre-breeding greylag geese," *Physiol Behav*, vol. 246, p. 113666, 2022.

[42] A. M. Zaki, S. K. Towfek, W. Gee, W. Zhang, and M. A. Soliman, "Advancing parking space surveillance using a neural network approach with feature extraction and dipper throated optimization integration," *Journal of Artificial Intelligence and Metaheuristics*, vol. 6, no. 2, pp. 16–25, 2023.

[43] T. Dokeroglu, E. Sevinc, T. Kucukyilmaz, and A. Cosar, "A survey on new generation metaheuristic algorithms," *Comput Ind Eng*, vol. 137, p. 106040, 2019.

[44] M. Braik, A. Sheta, and H. Al-Hiary, "A novel meta-heuristic search algorithm for solving optimization problems: capuchin search algorithm," *Neural Comput Appl*, vol. 33, no. 7, pp. 2515–2547, 2021.

[45] A. H. Halim, I. Ismail, and S. Das, "Performance assessment of the metaheuristic optimization algorithms: an exhaustive review," *Artif Intell Rev*, vol. 54, no. 3, pp. 2323–2409, 2021.

[46] D. S. Khafaga *et al.*, "An Al-Biruni earth radius optimization-based deep convolutional neural network for classifying monkeypox disease," *Diagnostics*, vol. 12, no. 11, p. 2892, 2022.

[47] A. A. Heidari, S. Mirjalili, H. Faris, I. Aljarah, M. Mafarja, and H. Chen, "Harris hawks optimization: Algorithm and applications," *Future generation computer systems*, vol. 97, pp. 849–872, 2019.

[48] S. L. Ayinla *et al.*, "Optimizing DC Motor Control via Leader Harris Hawks Algorithm with ITSE-ZLG Objective Function," in *2023 10th IEEE International Conference on Power Systems (ICPS)*, IEEE, 2023, pp. 1–6.

[49] Z. Liu, Y. Fang, L. Liu, and S. Ma, "A multi-leader Harris hawks optimizer with adaptive mutation and its application for modeling of silicon content in liquid iron of blast furnace," *Math Comput Simul*, vol. 213, pp. 466–514, 2023.

[50] S. Alzabeebee, A. A. Zuhaira, and R. K. S. Al-Hamd, "Development of an optimized model to compute the undrained shaft friction adhesion factor of bored piles," *Geomechanics and Engineering*, vol. 28, no. 4, pp. 397–404, 2022.

[51] M. Kumar, D. R. Kumar, J. Khatti, P. Samui, and K. S. Grover, "Prediction of bearing capacity of pile foundation using deep learning approaches," *Frontiers of Structural and Civil Engineering*, vol. 18, no. 6, pp. 870–886, 2024, doi: 10.1007/s11709-024-1085-z.

[52] M. Kumar, V. Kumar, B. G. Rajagopal, P. Samui, and A. Burman, "State of art soft computing based simulation models for bearing capacity of pile foundation: a comparative study of hybrid ANNs and conventional models," *Model Earth Syst Environ*, vol. 9, no. 2, pp. 2533–2551, 2023, doi: 10.1007/s40808-022-01637-7.